View metadata, citation and similar papers at core.ac.uk
brought to you by CORE
provided by University of Bedfordshire Repository

Making corrections to your proof

Please follow these instructions to mark changes or add notes to your proof. You can use Adobe Acrobat Reader (download the most recent version from **https://get.adobe.com**) or an open source PDF annotator.

For Adobe Reader, the tools you need to use are contained in **Annotations** in the **Comment** toolbar. You can also right-click on the text for several options. The most useful tools have been highlighted here. If you cannot make the desired change with the tools, please insert a sticky note describing the correction.

Please ensure all changes are visible via the 'Comments List' in the annotated PDF so that your corrections are not missed.

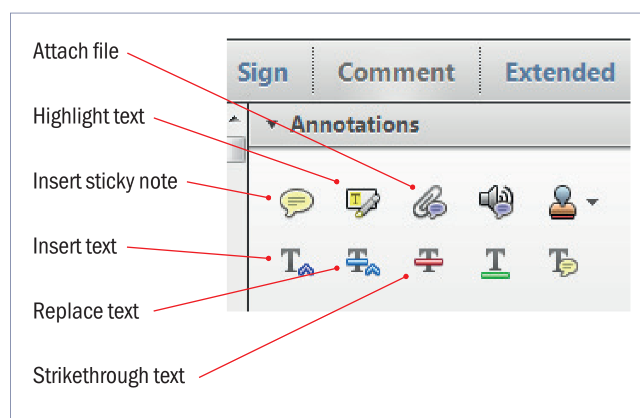

Do not attempt to directly edit the PDF file as changes will not be visible.

Replacing text

To replace text, highlight what you want to change then press the replace text icon, or right-click and press 'Add Note to Replace Text', then insert your text in the pop up box. Highlight the text and right click to style in bold, italic, superscript or subscript.

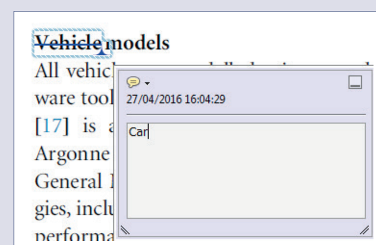

Inserting text

Place your cursor where you want to insert text, then press the insert text icon, or right-click and press 'Insert Text at Cursor', then insert your text in the pop up box. Highlight the text and right click to style in bold, italic, superscript or subscript.

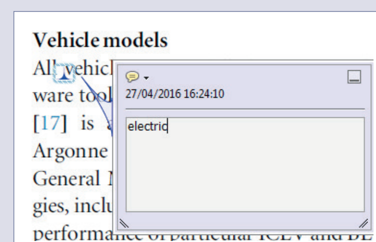

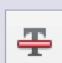

Deleting text

To delete text, highlight what you want to remove then press the strikethrough icon, or right-click and press 'Strikethrough Text'.

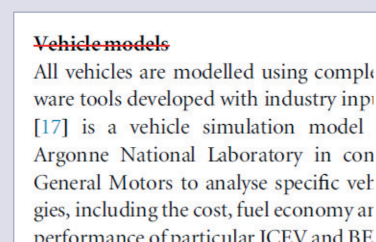

Highlighting text

To highlight text, with the cursor highlight the selected text then press the highlight text icon, or right-click and press 'Highlight text'. If you double click on this highlighted text you can add a comment.

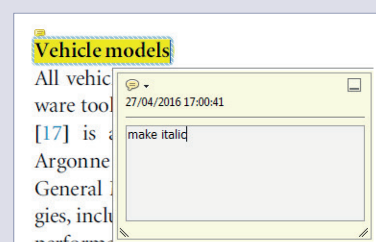

QUERY FORM

JOURNAL: Applied Physics Express

AUTHOR: M. Liu et al.

TITLE: Fast Fourier transport analysis of surface structures fabricated by laser interference lithography

ARTICLE ID: ab37ae

Your article has been processed in line with the journal style. Your changes will be reviewed by the Production Editor, and any amendments that do not comply with journal style or grammatical correctness will not be applied and will not appear in the published article.

The layout of this article has not yet been finalized. Therefore this proof may contain columns that are not fully balanced/ matched or overlapping text in inline equations; these issues will be resolved once the final corrections have been incorporated.

Please check that the **names of all authors as displayed in the proof are correct**, and that all **authors are linked to the correct affiliations**. Please also confirm that the correct corresponding author has been indicated. **Note that this is your last opportunity to review and amend this information before your article is published**.

If an explicit acknowledgment of funding is required, please ensure that it is indicated in your article. If you already have an Acknowledgments section, please check that the information there is complete and correct.

Please check that the funding information below is correct for inclusion in the article metadata

111 Project of China: No.D17017; National Key R&D Program of China: No.2016YFE0112100; Horizon 2020 Framework Programme: FabSurfWAR No.644971, NanoStencil No.767285; Jilin Provincial Science and Technology Program: No. 20190702002GH, No.20160623002TC, No.20180414002GH, No.20180414081GH, No.20180520203JH; National Natural Science Foundation of China: No.11504030.

Applied Physics Express **00**, 000000 (2019) **LETTER**
https://doi.org/10.7567/1882-0786/ab37ae

Fast Fourier transport analysis of surface structures fabricated by laser interference lithography

Mengnan Liu[1,2], Litong Dong[1,2,4], Ziang Zhang[1,2,4], Li Li[1,2], Lu Wang[1,2], Zhengxun Song[1,2], Zhankun Weng[1,2], Xueyan Han[1,2], Linhua Zhou[3*], and Zuobin Wang[1,2,4*]

[1]Ministry of Education Key Laboratory for Cross-Scale Micro and Nano Manufacturing, Changchun University of Science and Technology, Changchun 130022, People's Republic of China
[2]International Research Centre for Nano Handling and Manufacturing of China, Changchun University of Science and Technology, Changchun 130022, People's Republic of China
[3]Department of Applied Mathematics, Changchun University of Science and Technology, Changchun 130022, People's Republic of China
[4]IRAC & JR3CN, University of Bedfordshire, Luton LU1 3JU, United Kingdom

*E-mail: zhoulh@cust.edu.cn; wangz@cust.edu.cn

Received June 22, 2019; revised July 29, 2019; accepted August 1, 2019; published online MM DD, 2019

This paper presents an FFT (fast Fourier transform) analytical method for the study of surface structures fabricated by laser interference lithography (LIL). In the work, the FFT analytical method combined with Gaussian fitting is used to determine the periods and pattern distributions of surface structures from frequency spectra. For LIL, the processing parameters of incident and azimuth angles can be obtained corresponding to the period and pattern distribution. This work facilitates the detection of micro- and nano-structures, the analysis of pattern distribution in engineering, and the processing error analysis of LIL. © 2019 The Japan Society of Applied Physics

Periodic surface micro- and nano-structures are widely used for optimizing the properties of functional materials with controllable wettability,[1)] adhesion[2,3)] and reflectivity.[4–6)] Different technologies such as electron beam lithography (EBL),[7)] imprint lithography,[8)] self-assembly[9,10)] and laser interference lithography (LIL)[11–13)] have been developed to fabricate periodic surface micro- and nano-structures. Among the technolog uctures with different feature sizes on various materials. The spatial directions of periodic structures can be designed by the azimuth angles of incident beams. The azimuth angle is one of the important parameters in a LIL system, which directly defines the intensity distribution.[14)] The period of surface structures refers to the incident angles and wavelength.[15)] Obtaining the parameters from the images of surface patterns is important for processing error analysis and structure analysis.

The quality inspection of laser interference patterns has been studied for many years. Much work has been reported on this topic. Most surface measurements are focused on phase. It defines the structure position or orientation, and partly decides the quality of the structure. Different techniques have been developed for quality inspection based on phase analysis,[16,17)] such as phase-shifting interferometry (PSI) for deformation detection,[18,19)] phase unwrapping for holographic deformation analysis[20,21)] and fast phenomenon measurement.[22)] However, in LIL, the quality inspection of fabricated surface structures is dependent on traditional measurement tools. The current approach of periodic measurement relies mainly on the software functions of microscopes. Therefore, there is a need to find a more accurate way for the analysis of surface structures in LIL to determine the structure parameters and their corresponding parameters of interference patterns.

In this letter, we employ a fast Fourier transform (FFT) analytical method combined with Gaussian fitting for the study of periodic and multi-periodic surface patterns. We build a LIL system to fabricate micro- and nano-structures for analysis. The FFT analytical method is used to convert the structural data in the space domain into the frequency domain, and the incident and azimuth angles of interfering beams are determined by Gaussian fitting. An analytical model is established for the computing of the azimuth angles of two-beam, three-beam and four-beam LILs based on the fabricated surface structures. Periods of surface structures are obtained from frequency spectra (usually, the angular frequency spectra are called the frequency spectra). This analytical model can be used for the calibration and feedback of LIL system to correct optical setup errors. The parameters of the LIL are extracted by processing FFT analysis combined with Gaussian fitting on micro- and nano-structures. After obtaining the process parameters of LIL, the LIL system can be established to reconstruct functional micro- and nano-structures.

A general form of N-beam laser interference can be described as the superposition of electric field vectors of N beams ($\mathbf{E}_1$, $\mathbf{E}_2$, $\mathbf{E}_3$, …, $\mathbf{E}_N$), and the mth electric field vector can be written as

$$\boldsymbol{E_m} = A_m \boldsymbol{p_m} \cos(\boldsymbol{K_m} \cdot \boldsymbol{r} - \omega t + \varphi_m) \tag{1}$$

where A_m is the amplitude, $\mathbf{p}_m$ is the polarization vector, $\mathbf{K}_m$ is the propagation vector, $\mathbf{r}$ is the position vector, and φ_m is the initial phase.

The intensity distribution of N-beam interference field can be calculated by

$$|I(r)| = \sum_{m=1}^{N}\sum_{n=1}^{N} |E_m||E_n| \cos\langle E_m \cdot E_n \rangle. \tag{2}$$

After the FFT operation, I ($\boldsymbol{r}$) is converted into F ($\boldsymbol{L}$) which is

$$F(\boldsymbol{L}) = \iiint e^{-i\boldsymbol{L}\cdot\boldsymbol{r}} I(\boldsymbol{r}) d\boldsymbol{r}. \tag{3}$$

In LIL, the intensity distribution on the substrate is the same as that on the x-y plane. After the FFT operation, I (x, y) is converted into F (u, v), where u and v are a pair of variables. For simplified calculations, an orthogonal matrix "A" is used to place frequency spectra into the plane of x-y, which can be expressed as $\begin{pmatrix} u \\ v \end{pmatrix} = A \begin{pmatrix} y \\ x \end{pmatrix}$. The transformed expression is

 © 2019 The Japan Society of Applied Physics

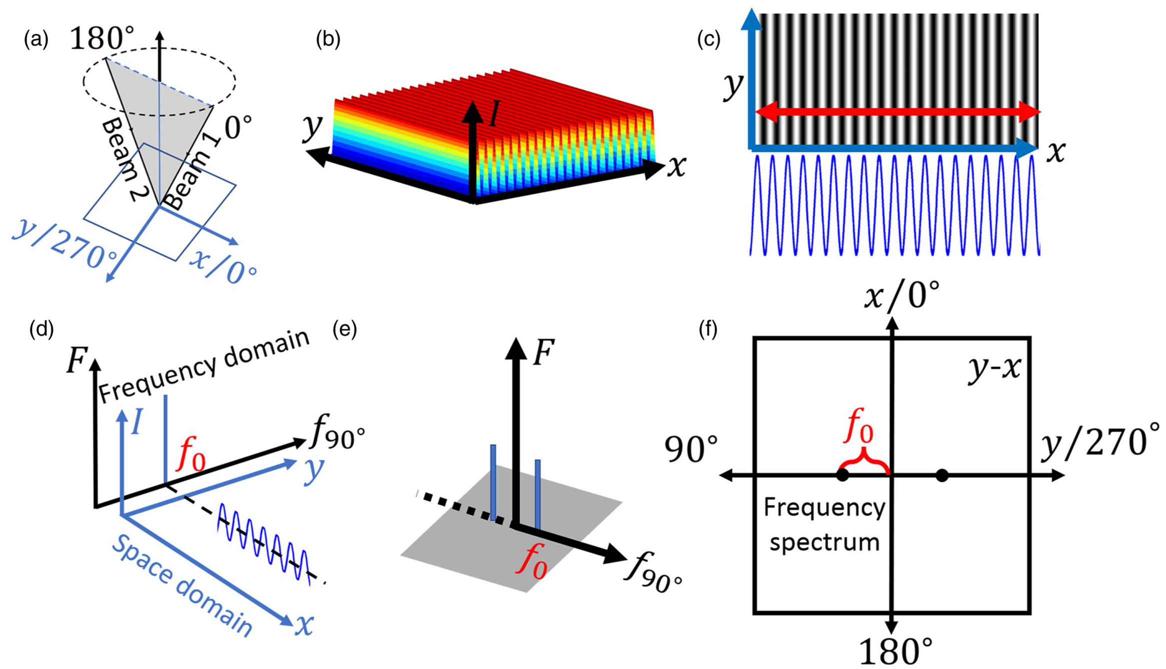

Fig. 1. (Color online) Schematic diagram of transforming the interference intensity into frequency spectra. (a) Two-beam interference configuration. (b) Spatial intensity distribution. (c) Intensity distribution on the *x*-*y* plane. (d) Schematic diagram of the mapping of the cosine function in the *x* axis direction on the frequency spectra. (e) Distribution of the cosine function in the *x* axis direction over the frequency spectra. (f) Frequency spectra of (c).

$$I(x, y) \overset{FFT}{\leftrightarrow} F(y, x). \tag{4}$$

The frequency distribution shows a 90° transpose between the frequency spectra and the *x*-*y* plane.

For analysis, the origin of frequency spectra is located at the center. The distribution of azimuth angles on the frequency spectra is analyzed by taking two-beam interference as an example, as shown in Fig. 1. On frequency spectra, the azimuth angle of 0° is placed at the 12 o'clock position on the unit circle and continues in the counterclockwise direction.

The azimuth angle can be regarded as located in the polar coordinates on the *x*-*y* plane, as shown in Fig. 1(a). Azimuth angles of incident beams are 0° and 180°, respectively. For patterns fabricated by LIL, Fig. 1(b) is the spatial distribution that is presented as a three-dimensional spatial distribution. The interference pattern on the *x*-*y* plane is used for processing FFT analysis. The intensity distribution shows a cosine distribution along the *x* axis, as shown in Fig. 1(c). For the frequency spectra of the cosine function without a constant term, the horizontal axis "$f_{90°}$" represents the frequency, and the vertical axis represents the value of the cosine function after processing FFT, as shown in Fig. 1(d). Because of the single frequency of Fig. 1(d), the frequency distribution along "$f_{90°}$" axis illustrates two central symmetry values of "F", as shown in Fig. 1(e). On the frequency spectrum of Fig. 1(c), the central symmetry values show a pair of symmetric points on the axis of 90° and 270° as shown in Fig. 1(f). The pair of black points of Fig. 1(f) demonstrates the frequency component. The "f_0" is the distance between the origin and the frequency component.

In this work, all images are converted to grayscale images and stored as uncompressed TIF files. After FFT processing, low-frequency pixels are placed at the image periphery. The program "fftshift" of MATLAB is used to place the low-frequency pixels at the origin or center part. When an image is processed by 2D FFT, the resulting frequency spectra contain the clusters of white pixels that are concentrated in a symmetrical circular pattern around the origin. The clusters of white pixels are the low-frequency signals which correspond to the background and the overall shape of the period distribution image. The high-frequency signal corresponds to the abrupt changes of pixel intensity which refers to the edge, noise and structural details. On the frequency spectra of grayscale images, low-frequency pixels are shown as white pixels, and high-frequency pixels are shown as black pixels.

In theoretical simulations, all incident beams are considered as Gaussian beams. Thus, low-frequency components are not symmetric white pixels but symmetric bright pixel fields. Gaussian fitting is used to obtain the center of symmetric bright pixel fields to perform FFT analysis.

The simulation interference patterns were generated by MATLAB to further explain the FFT analytical model. For simplicity, all incident beams had the same incident angle, intensity, polarization and wavelength. The incident beams were considered as Gaussian beams. Figure 2 shows the schemes of the interference configurations with different azimuth angles. Interference patterns are obtained on the substrates which correspond to the *x*-*y* plane.

Patterns under the three interference configurations and their frequency spectra with the same incident angles were generated by MATLAB as shown in Figs. 3(a)–3(c). Figure 3(d) shows multi-period patterns under the interference configuration of Fig. 2(c) with the incident angles of $\theta = \theta_1 = \theta_2 = \theta_3 \neq \theta_4$. All intensity distribution images were selected with the same size for analysis. Figures 3(e)–3(h) show the 3D frequency distributions of Figs. 3(i)–3(l) in the frequency domain to map the frequency distributions clearly.

© 2019 The Japan Society of Applied Physics

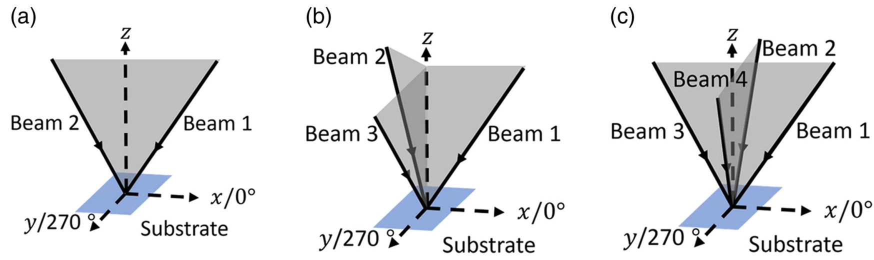

Fig. 2. (Color online) Interference configurations for processing FFT analysis. (a) Two-beam interference configuration with the azimuth angles of $\Phi_1 = 0°$ and $\Phi_2 = 180°$. (b) Three-beam interference configuration with the azimuth angles of, $\Phi_1 = 0°$, $\Phi_2 = 120°$ and $\Phi_3 = 240°$. (c) Four-beam interference configuration with the azimuth angles of $\Phi_1 = 0°$, $\Phi_2 = 90°$, $\Phi_3 = 180°$ and $\Phi_4 = 270°$.

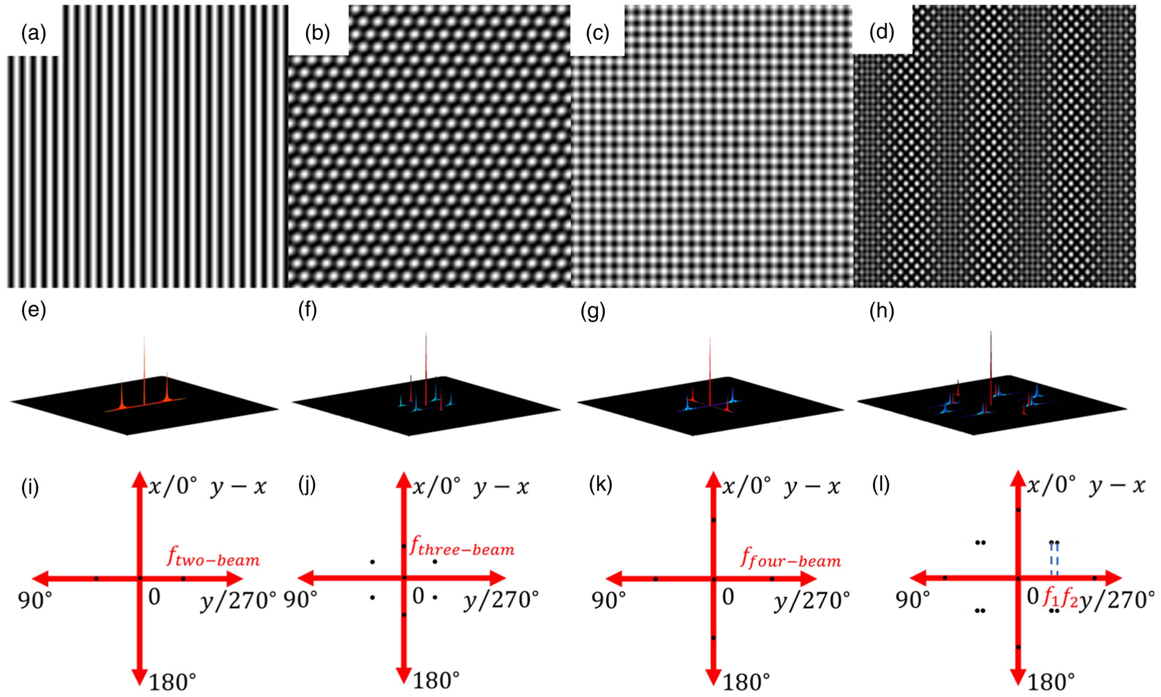

Fig. 3. (Color online) Schematic diagrams of interference intensity distributions and their spectral distributions on frequency spectra. (a)–(d) Simulation results of multi-beam LIL. (e)–(h) Frequency distributions of (a)–(d). (i)–(l) Schematic diagrams of frequency spectra corresponding to (e)–(h).

For two-beam, three-beam and four-beam laser interference, the intensity distributions on the x-y plane are shown in Figs. 3(a)–3(d). The intensity distributions are $I_{two\text{-}beam}$, $I_{three\text{-}beam}$, $I_{four\text{-}beam}$ and $I_{multi\text{-}period}$. After FFT, $I_{two\text{-}beam}$, $I_{three\text{-}beam}$ $I_{four\text{-}beam}$ and $I_{multi\text{-}period}$ are transformed into $F_{two\text{-}beam}$, $F_{three\text{-}beam}$, $F_{four\text{-}beam}$ and $F_{multi\text{-}period}$ which can be respectively expressed as

$$F_{two-beam} = 4\pi I_0 \delta(y)\delta(x) + \pi I_0 \delta(x) \times \begin{bmatrix} \delta(y - f_{two-beam}) \\ +\delta(y + f_{two-beam}) \end{bmatrix} \quad (5)$$

$$F_{three-beam} = I_0 \begin{Bmatrix} 6\pi\delta(y)\delta(x) \\ +4\pi^2\delta(x)\sum_{\beta=0,1}\delta(y + (-1)^\beta f_{three-beam}) \\ +8\pi\left[\sum_{\beta=0,1}\delta\left(x + (-1)^\beta \frac{1}{2} f_{three-beam}\right)\right] \\ \cdot\left[\sum_{\beta=0,1}\delta\left(x + (-1)^\beta \frac{3}{2} f_{three-beam}\right)\right] \end{Bmatrix} \quad (6)$$

$$F_{four-beam} = I_0 \begin{Bmatrix} 8\pi\delta(x)\delta(y) \\ -4\pi^2\delta(x)\sum_{\beta=0,1}\delta(y + (-1)^\beta f_{four-beam}) \\ -4\pi^2\delta(y)\sum_{\beta=0,1}\delta(x + (-1)^\beta f_{four-beam}) \end{Bmatrix} \quad (7)$$

$$F_{multi-period} = I_0 \begin{Bmatrix} 8\pi\delta(x)\delta(y) + 4\pi^2\delta(x)\sum_{\beta=0,1}\delta[y + (-1)^\beta(f_1 + f_2)] \\ +4\pi^2\left[\sum_{\beta=0,1}\delta(y + (-1)^\beta f_1)\right]\left[\sum_{\beta=0,1}\delta(x + (-1)^\beta f_1)\right] \\ +4\pi^2\left[\sum_{\beta=0,1}\delta(y + (-1)^\beta f_1)\right]\left[\sum_{\beta=0,1}\delta(x + (-1)^\beta f_2)\right] \\ +4\pi^2\left[\sum_{\beta=0,1}\delta(y + (-1)^\beta f_2)\right]\left[\sum_{\beta=0,1}\delta(x + (-1)^\beta f_1)\right] \\ +4\pi^2\left[\sum_{\beta=0,1}\delta(y + (-1)^\beta f_2)\right]\left[\sum_{\beta=0,1}\delta(x + (-1)^\beta f_2)\right] \\ +8\pi^2\delta(y)\sum_{\beta=0,1}\delta(x + 2(-1)^\beta f_2) \end{Bmatrix}. \quad (8)$$

 © 2019 The Japan Society of Applied Physics

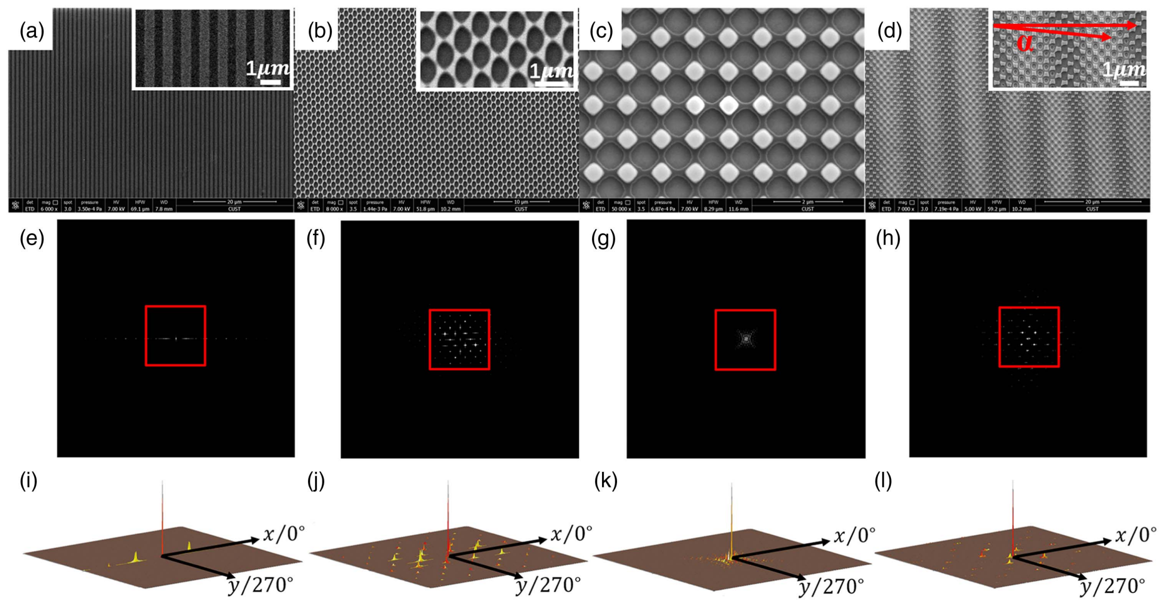

Fig. 4. (Color online) SEM images of periodic structures fabricated by LIL and their frequency spectra. (a)–(d) The SEM images of the structures. (e)–(h) Frequency spectra with 747 × 747 pixels of (a)–(d). (i)–(l) Marked areas of (e)–(h).

According to Eqs. (5)–(8), the results of Dirac function show three, seven, five and thirteen coordinates with the origin and pairs of symmetric coordinates. The distance between the origin and the coordinate are the frequencies of $I_{two\text{-}beam}$, $I_{three\text{-}beam}$ $I_{four\text{-}beam}$ and $I_{multi\text{-}period}$. The origin corresponds to the constant terms of Eqs. (5)–(8), which illustrates the central peak, as shown in Figs. 3(e)–3(h). The symmetric coordinates correspond to the frequency distributions along the azimuth angles on the frequency spectra, as shown in Figs. 3(i)–3(l).

For the above analysis, the following conclusions can be obtained. On the frequency spectra of periodic patterns, the frequency components of periodic structures show the origin and several pairs of symmetric coordinates. Half components of the pairs of symmetric coordinates contain the information for analysis. The frequency corresponds to the distance between the origin and one frequency component in the frequency spectra. The direction of a pair of symmetric components shows one azimuth angle of the periodic structure distributions, as shown in Figs. 3(i)–3(l). The FFT result is unaffected by sampling area.

In the experiment, periodic structures were fabricated via multi-beam LIL. The single-mode diode-pumped solid-state (DPSS) laser (MSL-FN-360-S, CNI) with the wavelength of 360 nm was used to build the LIL system. The multi-beam LIL can directly create a variety of periodic patterns on positive photoresist (AR-P 3740, Allresist). The scanning electron microscope (SEM; Quanta250, FEI) was employed to evaluate the periodic structures, and the SEM images with the size of 1536 × 1103 pixels were stored as uncompressed TIF files for performing FFT analysis. Limited by image size, all SEM images were cut into 747 × 747 pixels for analysis from the center. Two-beam, three-beam and four-beam LIL systems were established to generate the periodic structures for error analysis.

Due to the different modification thresholds of materials, the frequency distribution over the spectra would be distributed multiple times in the same period. In the experiment, the nearest distribution of frequency spectra was used to obtain the real period of the fabricated structures and the azimuth angle distributions of the interference beams.

The structures fabricated by two-beam, three-beam and four-beam LIL were used to perform the FFT analysis, as shown in Fig. 4. Figures 4(a)–4(d) are the SEM images of the structures. After cutting the images of Figs. 4(a)–4(d) into 747 × 747 pixels from the center, programs "fftshift" and "fft" were used for obtaining the central location of each frequency component from frequency spectra images, as shown in Figs. 4(e)–4(h). Figures 4(i)–4(l) are the marked areas of Figs. 4(e)–4(h), which show the distributions of frequency components.

The periodic structure of Fig. 4(a) is fabricated by two-beam LIL according to $I_{two\text{-}beam}$ with the theoretical period of 1 μm (corresponding to the incident angle of 0.18°). The scale of Fig. 4(a) is 20.00 μm corresponding to 446 pixels. Gaussian fitting was used to obtain the center of each bright-field in Fig. 4(e). The period calculated from the frequency distribution in Fig. 4(e) is 1.06 μm (corresponding to the incident angle of 0.17°), and there are two beams that are axisymmetric with the azimuth angle of 90°. The azimuth angle is the same as the theoretical value. The actual incident angle is 0.01° smaller than the theoretical value.

The periodic structure of Fig. 4(b) is fabricated by three-beam LIL according to $I_{three\text{-}beam}$ with the theoretical period of 1.00 μm (corresponding to the incident angle of 0.43°). The scale of Fig. 4(b) is 10.00 μm corresponding to 298 pixels. Gaussian fitting is used to obtain the center of each bright-field in Fig. 4(f). The period calculated from the frequency distribution in Fig. 4(f) is 1.03 μm (corresponding to the incident angle of 0.42°), and there are three incident beams with the azimuth angles of $\Phi_1 = 0.00°$, $\Phi_2 = 161.00°$ and $\Phi_3 = 260.07°$. The actual incident angle is 0.01° smaller than the theoretical value. The errors of azimuth angles are 41.00° and 20.07°. One of the main difficulties in the construction of the asymmetrical spatial structure of the optical setup is to determine the position of the azimuth angles.

© 2019 The Japan Society of Applied Physics

The periodic structure of Fig. 4(c) is fabricated by four-beam LIL according to $I_{four\text{-}beam}$ with the theoretical period of 1.00 μm (corresponding to the incident angle of 0.18°). The scale of Fig. 4(c) is 2.00 μm corresponding to 372 pixels. Gaussian fitting is used to obtain the center of each bright-field in Fig. 4(g). The period calculated from the frequency distribution in Fig. 4(g) is 0.99 μm, and there are four incident beams with azimuth angles of $\Phi_1 = 0.00°$, $\Phi_2 = 90.00°$, $\Phi_3 = 180.00°$ and $\Phi_4 = 270.00°$. There is an error of 0.01 μm between the theoretical period and calculated period.

The periodic structure of Fig. 4(d) is fabricated by four-beam LIL according to Eq. (7), with the theoretical azimuth angles of $\Phi_1 = 0.00°$, $\Phi_2 = 90.00°$, $\Phi_3 = 180.00°$ and $\Phi_4 = 270.00°$. The periods of 720.00 nm, 770.88 nm, and 10.59 μm (corresponding to the incident angles of $\theta_2 = \theta_3 = \theta_4 = 13.50°$ and $\theta_1 = 15.50°$). The scale of Fig. 4(c) is 20.00 μm corresponding to 520 pixels. Gaussian fitting is used to obtain the center of each bright-field in Fig. 4(h). The periods calculated from the frequency distribution in Fig. 4(h) are 10.36 μm, 747.16 nm and 754.39 nm, and there are four incident beams with the azimuth angles of $\Phi_1 = 0.00°$, $\Phi_2 = 180°$, $\Phi_3 = 275.57°$ and $\Phi_4 = 95.57°$. Compared with the theoretical image, the error of azimuth angle shows an angle difference of 5.57° (which is the angle of α) on the structure distribution, as shown in Fig. 4(d).

By processing the FFT analytical model, azimuth angles and periods of Figs. 4(a)–4(d) show different results with their theoretical values. The azimuth angle and period errors reflect the deviations during the construction of the LIL system. The deviation of the spatial angle of the optical setup is difficult to measure accurately. For the above analysis, the real azimuth angle of Figs. 4(b)–4(d) show different values from theoretical azimuth angles. The error is caused by misalignments of optical components during the manual setup of the LIL system. Due to errors generated by manual measurement methods, the periods of Figs. 4(a)–4(d) show different values from theoretical periods. This FFT analytical method calculates the parameters of the structure based on the pixel distribution of the image, which is not affected by structural scale changes. This approach is more accurate than the measurement function that comes with the existing software.

To conclude, we present an approach to obtain surface features of ordered structures and corresponding process parameters of LIL via FFT analysis combined with Gaussian fitting. The FFT analytical model is established for computing the azimuth angles and periods of the ordered micro- and nano-structures fabricated by LIL. The analytical model can be used for error detection and analysis in the process of micro- and nano-structure manufacturing. Comparing with traditional measurements, the process parameters of micro- and nano-structures, including the period, duty ratio and height, are calculated precisely through FFT analysis. On one hand, this work provides a method for the real-time error analysis and error corrections of LIL systems from interference pattern intensity distributions. On the other hand, this work provides a way to replicate functional patterns of animals and plants by the FFT analytical method for the fabrication of biomimetic structures with LIL. After calculating the periods and azimuth angles from the frequency spectra, the parameters can be used to build LIL systems to replicate the structures on other materials.

Acknowledgments National Key R&D Program of China (No.2016YFE0112100); EU H2020 Program (FabSurfWAR No.644971; NanoStencil No.767285); National Natural Science Foundation of China (No.11504030); Jilin Provincial Science and Technology Program (Nos.20160623002TC, 20180414002GH, 20180414081GH, 20180520203JH and 20190702002GH); "111" Project of China (D17017).

1) A. Marmur., Langmuir **20**, 3517 (2004).
2) L. Feng, Y. Zhang, J. Xi, Y. Zhu, N. Wang, F. Xia, and L. Jiang, Langmuir **24**, 4114 (2008).
3) D. Wang, Z. Wang, Z. Zhang, Y. Yue, D. Li, R. Qiu, and C. Maple, J. Appl. Phys. **115**, 233101 (2014).
4) H.-W. Park, S. Ji, H. Lim, D.-W. Choi, J.-S. Park, and K.-B. Chung, J. Appl. Phys. **109**, 121604 (2016).
5) S. Z. Oener, J. van de Groep, B. Macco, P. C. P. Bronsveld, W. M. M. Kessels, A. Polman, and E. C. Garnett, B, Nano. Lett. **16**, 3689 (2016).
6) I. Khan, M. Bauch, T. Dimopoulos, and J. Dostalek, Nanotechnology **28**, 325201 (2017).
7) J. Martin and J. Plain, J. Phys. D: Appl. Phys. **48**, 184002 (2015).
8) Itsunari Yamada and Y. Ishihara, Jpn. J. Appl. Phys. **9**, 052202 (2016).
9) Q. Haimei Zheng, F. Zhan, M. Zavaliche, F. Sherburne, M. P. Straub, L.-Q. Cruz, Chen, Uli Dahmen, and R. Ramesh, Nano Lett. **6**, 1401 (2006).
10) J. Yeom et al., Nat. Mater. **14**, 66 (2014).
11) D. Wang, Z. Wang, Z. Zhang, Y. Yue, D. Li, and C. Maple, Appl. Phys. Lett. **102**, 081903 (2013).
12) Y. Kaganovskiia, H. Vladomirsky, and M. Rosenbluh, J. Appl. Phys. **100**, 044317 (2006).
13) D. Xia, Z. Ku, S. C. Lee, and S. R. J. Brueck, Adv. Mater. **23**, 147 (2011).
14) Z. Zhang, L. Dong, Y. Ding, L. Li, Z. Weng, and Z. Wang, Opt. Express **25**, 29135 (2017).
15) D. Wang, Z. Wang, Y. Yue, J. Yu, C. Tan, D. Li, R. Qiu, and C. Maple, Optik **126**, 2902 (2015).
16) F. Sawaf and R. M. Groves, Appl. Optics. **53**, 5439 (2014).
17) J. Dong, C. Jiang, and S. Jia, Opt. Lett. **41**, 4301 (2016).
18) Chao Tian and S. Liu, Opt. Express **24**, 18695 (2016).
19) Y. Zhang, X. Tian, and R. Liang, Opt. Express **25**, 26554 (2017).
20) J. T. Judge, C. Quan, and P. J. Bryanston-Cross, Opt. Eng. **31**, 533 (1992).
21) R. Guo, W. Zhang, R. Liu, C. Duan, and F. Wang, Opt. Lett. **43**, 3449 (2018).
22) Haixia Wang and Q. Kemao, Opt. Express **25**, 32669 (2017).

 © 2019 The Japan Society of Applied Physics